

# A Novel Method for Improving LEO Kinematic Real-Time Precise Orbit Determination With Neural Networks

Wei Zhang<sup>ID</sup>, Keke Zhang<sup>ID</sup>, Xingxing Li<sup>ID</sup>, Jiaqi Wu<sup>ID</sup>, Yongqiang Yuan<sup>ID</sup>, and Yuanchen Fu<sup>ID</sup>

**Abstract**—The kinematic approach [i.e., kinematic precise point positioning (PPP)] has been extensively employed in real-time precise orbit determination (RTPOD) of low Earth orbit (LEO) satellites. Nonetheless, this approach typically suffers from a degraded accuracy and robustness due to its sensitivity to global navigation satellite system (GNSS) ephemeris errors and observation quality/geometry. To address this issue, we propose a novel method that incorporates the backpropagation neural network (BPNN) model into LEO kinematic RTPOD (KRTPOD) to improve its accuracy and robustness. The historical KRTPOD results are compared with external orbit products to compute orbit errors. Meanwhile, multiple features are generated from the historical KRTPOD processing. We train the BPNN model to discover the nonlinear relationship between these features and orbit errors. Based on the trained model, orbit errors of LEO KRTPOD can be forecast according to the input features and then serve as the orbit compensation to improve LEO orbits in real time. Data throughout 2022 from six LEO satellites are processed to examine the performance of this method. Our findings reveal that the proposed method can significantly improve the accuracy of LEO KRTPOD by up to 39.0%. Benefiting from this method, a promising accuracy of 3.2 cm can be achieved in LEO KRTPOD. We also demonstrate the superior generalization ability of the new method under different scenarios. Moreover, this method can enhance the robustness of LEO KRTPOD by mitigating the contamination caused by large GNSS ephemeris errors and accelerating convergence.

**Index Terms**—Backpropagation neural networks (BPNNs), global navigation satellite system (GNSS), kinematic approach, low Earth orbit (LEO) satellites, real-time precise orbit determination (RTPOD).

## I. INTRODUCTION

THE ever-growing demand for high-precision and low-latency location service has brought global navigation satellite system (GNSS) to the forefront of current research and also poses challenge to the traditional GNSS-based navigation [1], [2]. As the main positioning technique in GNSS domains, precise point positioning (PPP) can achieve the

Manuscript received 19 March 2024; revised 15 June 2024; accepted 1 July 2024. Date of publication 16 July 2024; date of current version 22 July 2024. This work was supported in part by the National Key Research and Development Program of China under Grant 2021YFC3000504; in part by the National Natural Science Foundation of China under Grant 41974027, Grant 42204017, and Grant 42374015; and in part by the National Funded Postdoctoral Researcher Program, China, under Grant GZB20230537. The Associate Editor coordinating the review process was Dr. Yulong Huang. (*Corresponding author: Keke Zhang*)

The authors are with the School of Geodesy and Geomatics, Wuhan University, Wuhan 430079, China (e-mail: kkzhang@whu.edu.cn).

Digital Object Identifier 10.1109/TIM.2024.3427853

centimeter-level accuracy with a single receiver. However, it typically requires a long initialization time (tens of minutes) [3], potentially limiting its real-time application. The rapid advancement of low Earth orbit (LEO) satellites in recent years provides an effective solution to this limitation. Compared with GNSS satellites in medium/high orbits, LEO satellites offer some pronounced advantages such as the lower altitude for delivering stronger signals, faster motion for rapid change of geometric distribution, and larger inclination for wider coverage [4], [5]. By virtue of these advantages, LEO-augmented navigation has attracted unprecedented attention recently and is becoming a promising technique for future navigation.

An essential prerequisite for LEO-augmented navigation is that the locations of LEO satellites, that is, LEO orbits, are precisely known. Typically, LEO orbits with an accuracy of 1–2 cm can be determined using precise orbit/clock products of GNSS satellites in post processing [6], [7]. These postprocessed orbits of LEO satellites, however, can only be obtained with the latency of a few days to a few weeks due to the delay of GNSS final precise orbit/clock products. To meet the requirements of LEO-augmented navigation in time-critical scenarios, there is a pressing need for precise orbits of LEO satellites with low latency and even no latency. It is, therefore, of vital importance to investigate real-time precise orbit determination (RTPOD) of LEO satellites.

With the support of LEO onboard GNSS observations, there are two approaches, that is, the reduced-dynamic approach and the kinematic approach, commonly employed to realize LEO RTPOD. The former one makes full use of LEO onboard GNSS observations and satellite dynamic information to determine LEO orbits [8], [9]. As a result, the derived orbits are less affected by imperfect geometrical information (e.g., measurement outliers). In addition, the orbits can maintain accuracy and continuity even in the absence of observations for a short time. With this method, the accuracy of LEO real-time orbits is at decimeter to meter level based on GNSS broadcast ephemerides [10], [11], [12], [13]. By using GNSS real-time orbit/clock products provided by the international GNSS service (IGS) real-time service (RTS), the orbit accuracy can reach centimeter level [14], [15], [16]. The reduced-dynamic approach, however, generally presents a strong dependence on the accuracy of the dynamic parameters and might lead to a significantly deteriorated accuracy of LEO RTPOD during orbital maneuvers [17]. Besides, the introduction of satellite dynamic information, such as gravitational perturbation and

empirical accelerations, raises a high demand for computational resources.

For onboard processing of LEO RTPOD with limited computational resources, the kinematic approach has aroused greater concern in recent years. Different from the reduced-dynamic approach, the kinematic approach (i.e., kinematic PPP) exclusively uses onboard GNSS observations with no consideration of dynamic information [18]. Thereby, this method is free of the aberrant dynamic information particularly during orbital maneuvers. Additionally, it can effectively conserve computational resources due to its simple observation model. This makes the kinematic approach more suited for onboard processing than the reduced-dynamic approach [19]. These benefits make the kinematic approach a representative and irreplaceable method in LEO RTPOD. With this method, a 3-D accuracy around 0.7 m can be achieved for the single-frequency RTPOD solution of SJ-9A satellite [20]. Benefiting from the availability of real-time orbit/clock products from the Center National d'Etudes Spatiales (CNES), a 3-D root mean square (rms) error around 11 cm can be obtained in the kinematic RTPOD (KRTPOD) of GRACE-A/B satellites [16]. By fixing the phase ambiguities to integer, the 3-D rms of orbit differences (OD) can be reduced from 7.2 to 5.2 cm for the KRTPOD of Sentinel-3A satellite [21]. Nonetheless, the kinematic approach typically presents a high sensitivity to GNSS ephemeris errors and observation geometry/quality due to the sole use of onboard GNSS observations. This leads to a lower accuracy and robustness of LEO KRTPOD compared to the reduced-dynamic RTPOD [16], thus potentially hampering its practical use.

In this study, we mainly focus on improving the accuracy as well as the robustness of LEO KRTPOD. Different from the previous literature, we propose a novel method where the orbit errors of LEO KRTPOD are modeled and subsequently utilized to compensate for LEO orbits in real time. The key of this method lies in the modeling of LEO real-time orbit errors. These orbit errors, however, typically show a strong nonlinearity and complexity and remain challenging to be described accurately using the mathematical models. Ongoing advancements in machine learning technology along with its extensive applications in data science particularly in the modeling of complex and nonlinear systems presently provide us with a promising solution to this issue [22], [23]. We adopt the backpropagation neural networks (BPNNs), a type of machine learning algorithm, to conduct the orbit error modeling in this method [24]. This selection is motivated by some notable advantages of the BPNN model such as the remarkable capability of modeling complex nonlinear relationships and the excellent generalization ability [25]. More importantly, compared with other neural network models, the BPNN model is distinguished by its simple implementation and fast speed of the training/testing procedure. These advantages endow the new method with great potential to improve the accuracy and robustness of LEO KRTPOD with no significant sacrifice of computational efficiency. As such, our new method might be promisingly implemented in engineering domains with high-efficiency requirement and limited computational resources in the future, particularly for onboard processing.

With the BPNN model, our new method is aimed at modeling the orbit errors and improving the accuracy and robustness of LEO KRTPOD. The primary contributions of this article are highlighted as follows.

- 1) To address the issue of the degraded accuracy and robustness of LEO KRTPOD, we propose a novel method that introduces neural networks into LEO KRTPOD for the first time to improve its accuracy and robustness. We train the BPNN model to map the nonlinear relationships between multiple features and orbit errors. During the processing of KRTPOD, the modeled orbit errors serve as the compensation for LEO real-time orbits.
- 2) Tests on different LEO satellites show that this method can ensure a notably improved accuracy of LEO KRTPOD even using different GNSS ephemerides. In addition, this method can enhance the robustness of LEO KRTPOD by significantly mitigating the contamination caused by large GNSS ephemeris errors and shortening the convergence time.
- 3) We design multiple solutions to validate the generalization ability of this method. Tests reveal that the accuracy of KRTPOD for one LEO satellite can still be significantly improved even using the trained model from another LEO satellite. It demonstrates the superior generalization ability of our new method.

The remainder of this article is organized as follows: Section II provides a detailed description of the proposed method. Afterward, the datasets and processing strategies are introduced in Section III. Section IV presents and analyzes the experimental results based on the proposed method. Additionally, we make a discussion about the pros and cons of the proposed method in LEO KRTPOD in Section V. Finally, the summary and conclusions are given Section VI.

## II. METHODOLOGY

### A. Principles of the Proposed Method

The framework of the proposed method has been displayed in Fig. 1. The method comprises three parts: 1) KRTPOD processing; 2) model training; and 3) model forecasting. For the KRTPOD processing part, GNSS real-time orbit/clock products (broadcast ephemerides or precise ephemerides) and LEO onboard GNSS observations (code and carrier phase) are collected first; then the data preprocessing is conducted. We employ the “TurboEdit” algorithm to detect the cycle slip of carrier phase and remove the outliers [26]. Afterward, the observation equations can be constructed as follows:

$$\begin{cases} P_i = \rho + c(\delta_r - \delta^s) + c(b_{r,i} - b_i^s) + \frac{\lambda_i^2}{\lambda_1^2} I_1 + \varepsilon_{P_i} \\ L_i = \rho + c(\delta_r - \delta^s) + c(B_{r,i} - B_i^s) - \frac{\lambda_i^2}{\lambda_1^2} I_1 + \lambda_i N_i + \varepsilon_{L_i} \end{cases} \quad (1)$$

where  $P$  and  $L$  denote the raw code and carrier phase observations, respectively.  $s, r$ , and  $i$  indicate the GNSS satellite, LEO receiver, and the frequency, respectively.  $\rho$  denotes the geometry distance between LEO receiver and GNSS satellite.

$c$  is the light speed in vacuum.  $\delta_r$  and  $\delta^s$  indicate the clock offset of LEO receiver and GNSS satellite, respectively.  $b_{r,i}$  and  $b_i^s$  indicate the code bias at the LEO receiver and GNSS satellite sides, respectively, whereas  $B_{r,i}$  and  $B_i^s$  are their carrier-phase counterparts.  $\lambda_1$  and  $\lambda_i$  are the wavelength of the first frequency and the  $i$ th frequency, respectively.  $I_1$  indicates the ionospheric delay of the first frequency.  $N_i$  is the phase ambiguity of the  $i$ th frequency.  $\varepsilon_{P_i}$  and  $\varepsilon_{L_i}$  are the measurement noise of the code and carrier phase observations, respectively.

To eliminate the impact caused by the first-order ionospheric delay on the KRTPOD results, we employ the ionosphere-free (IF) combination observations as follows:

$$\begin{cases} P_{\text{IF}} = \frac{f_1^2}{f_1^2 - f_2^2} P_1 - \frac{f_2^2}{f_1^2 - f_2^2} P_2 \\ L_{\text{IF}} = \frac{f_1^2}{f_1^2 - f_2^2} L_1 - \frac{f_2^2}{f_1^2 - f_2^2} L_2 \end{cases} \quad (2)$$

where  $f_1$  and  $f_2$  denote the frequency values of GNSS signals. By combining (1) and (2), we have

$$\begin{cases} P_{\text{IF}} = \rho + c(\delta_r - \delta^s) + c(b_{r,\text{IF}} - b_{\text{IF}}^s) + \varepsilon_{P_{\text{IF}}} \\ L_{\text{IF}} = \rho + c(\delta_r - \delta^s) + c(B_{r,\text{IF}} - B_{\text{IF}}^s) + \lambda_{\text{IF}} N_{\text{IF}} + \varepsilon_{L_{\text{IF}}} \end{cases} \quad (3)$$

in which  $P_{\text{IF}}$  and  $L_{\text{IF}}$  denote the IF code and carrier phase observations, respectively.  $b_{r,\text{IF}}/B_{r,\text{IF}}$  and  $b_{\text{IF}}^s/B_{\text{IF}}^s$  indicate the IF code/carrier-phase bias at the LEO receiver and GNSS satellite sides, respectively.  $\lambda_{\text{IF}}$  indicates the IF wavelength.  $N_{\text{IF}}$  is the phase ambiguity of the IF combination.  $\varepsilon_{P_{\text{IF}}}$  and  $\varepsilon_{L_{\text{IF}}}$  are the IF noise of the code and carrier phase observations, respectively.

We further linearize the observation equations (3) and obtain the error equations as follows:

$$\begin{cases} p_{\text{IF}} = \mu_r^s \cdot x + c(\hat{\delta}_r - \hat{\delta}^s) + \varepsilon_{P_{\text{IF}}} \\ l_{\text{IF}} = \mu_r^s \cdot x + c(\hat{\delta}_r - \hat{\delta}^s) + \lambda_{\text{IF}} \hat{N}_{\text{IF}} + \varepsilon_{L_{\text{IF}}} \end{cases} \quad (4)$$

in which  $p_{\text{IF}}$  and  $l_{\text{IF}}$  indicate the observed-minus-computed (OMC) code and carrier phase observations, respectively.  $\mu_r^s$  is the unit vector from LEO receiver to GNSS satellite.  $x$  denotes the position correction of LEO receiver.  $\hat{\delta}_r$  indicates the clock offset correction of LEO receiver biased by the receiver code bias.  $\hat{N}_{\text{IF}}$  contains the IF phase ambiguity and the code/carrier-phase bias.  $\hat{\delta}^s$  indicates the clock offset of GNSS satellite biased by the satellite code bias, which can be eliminated by GNSS clock products. Thus, the estimated parameters will be

$$X = (x, \hat{\delta}_r, \hat{N}_{\text{IF}}). \quad (5)$$

It is noteworthy that the intersystem bias parameters should also be estimated provided that multi-GNSS observations are used. A recursive least squares estimator is adopted to perform the estimation from which we can obtain the epochwise positions of LEO satellite in real time. Meanwhile, multiple epochwise features related to LEO real-time orbits are also generated from the estimation as displayed in Table I. These features comprise three parts, that is, the priori information, the observation information, and the posterior information. The prior information refers to the priori values of the estimated parameters such as the priori positions of LEO receiver and the priori clock offset of LEO receiver. The

TABLE I  
FEATURE SETS GENERATED FROM LEO KRTPOD PROCESSING

Features	Abbreviation
Epoch	Epo
Number of observations	Nobs
LEO priori coordinates	PX, PY, PZ
Estimated corrections of LEO coordinates	dX, dY, dZ
LEO priori clock offsets	Clk
Estimated correction of LEO clock offsets	dClk
Posterior residuals of phase and code	LC, PC
Elevation	Ele
Mean square error of LEO coordinates	SigX, SigY, SigZ
Parameter covariance of LEO coordinates	QXX, QXY, QXZ, QYY, QYZ, QZZ
Mean square error of unit weight	Sig0

observation information includes the observation epoch, the number of observations, and the elevation angle. These two parts can be obtained from (3) before the estimation. The posterior information represents the posterior results generated from the estimation, such as the estimated corrections of LEO positions and the mean square error of unit vector. This part can be obtained after the solution of (5). These features are theoretically related with the estimation accuracy of LEO positions and will compose the feature sets for model training/testing. The KRTPOD processing is performed on the GNSS+ REsearch, Application and Teaching (GREAT) software that was designed and developed at the School of Geodesy and Geomatics of Wuhan University [27].

The model training part is aimed at generating a BPNN model to describe the relationship between the input and output as accurately as possible. Within this study, the input involves multiple features related to orbit errors from the historical processing of LEO KRTPOD (see Table I). Meanwhile, the corresponding generated real-time orbits are compared with external precise orbit products to compute orbit errors that will serve as the output of the model.

The BPNN model typically consists of three parts: input layer, hidden layer, and output layer. The input layer receives the input features and convey them to the hidden layer. The hidden layer part comprises one or more layers, each of which is composed of multiple neurons. These layers/neurons are responsible for extracting features from the input data and building the nonlinear relationship between the input and the output. To enhance the nonlinearity of the model, the activation function is indispensable. Herein, we select a representative activation function, the rectified linear unit (ReLU) function [28], to achieve the nonlinearity enhancement of the model. This selection is motivated by its high computational efficiency and sparse activation. The ReLU function can be expressed as follows:

$$\sigma(x) = \max(x, 0) \quad (6)$$

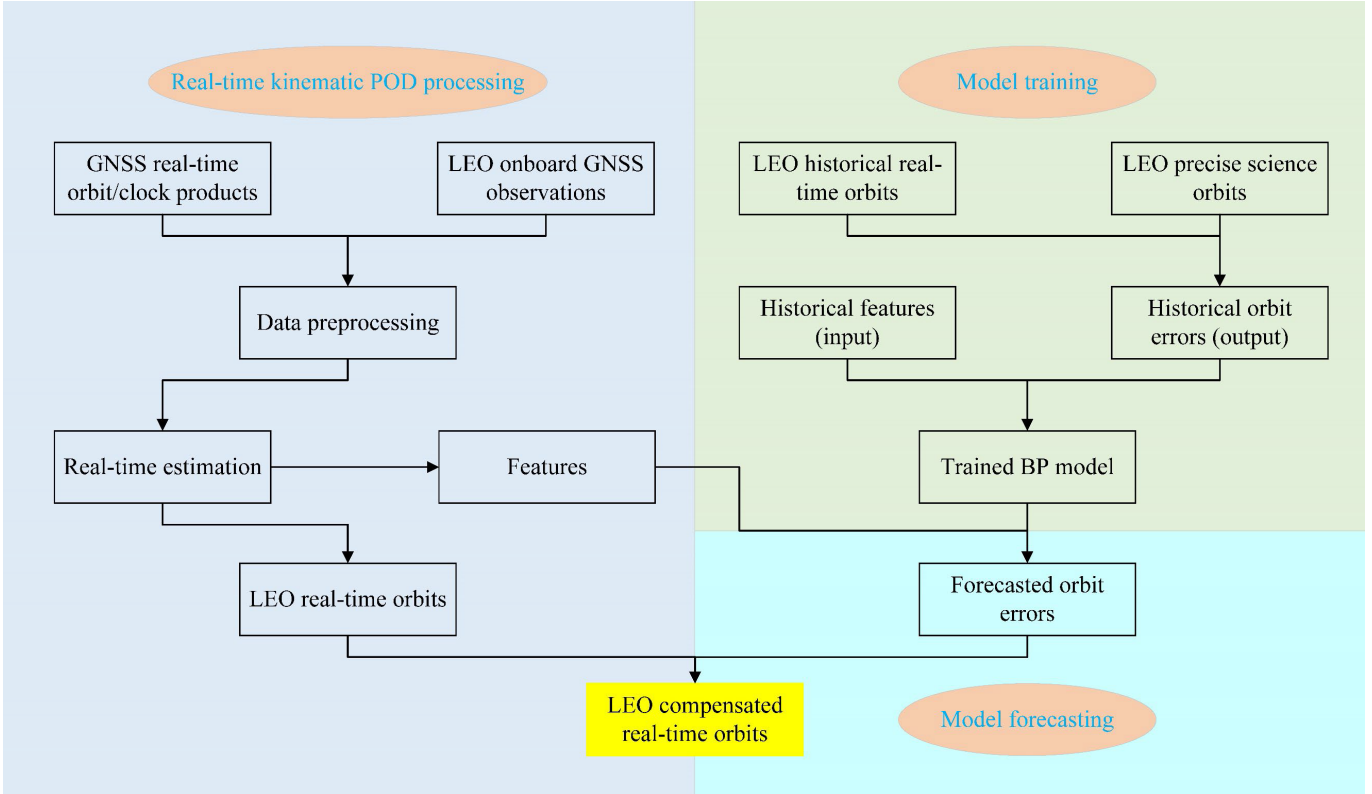


Fig. 1. Framework of the proposed method.

where  $\max(\cdot)$  indicates the maximum value in 0 and  $x$ . After a complete forward propagation, the model output can be obtained. A loss function is then applied to evaluate the approximation between the model output and the true output. Since the objective of the model training is to obtain the model parameters that minimize the value of the loss function, a back propagation is subsequently conducted to compute the gradients of the loss value with respect to the model parameters. With these gradients, the model parameters can be updated and then employed in the next forward/back propagation. After several iterations of the forward/back propagation processing, a trained model with the optimal model parameters can be obtained.

Based on the trained BPNN model, the generated features from the KRTPOD processing part will be used to forecast the orbit errors. After that, the forecast orbit errors will serve as the compensation for LEO real-time orbits to improve the accuracy. It is worth noting that the model training can be accomplished using historical datasets before the KRTPOD processing part. In this case, the model forecasting can be realized nearly with no latency. Therefore, this proposed method, on the one hand, is of great potential to improve the accuracy of LEO KRTPOD. On the other hand, it causes no diminution of the computational efficiency in RTPOD processing and can be implemented in real time.

### B. Evaluation Metrics

Since our concentration of this study is on improving the accuracy of LEO KRTPOD using the proposed method,

a preferred option of the evaluation metrics will be the accuracy assessment of the improved orbits. This is achieved by the comparison between our improved orbits and external precise science orbit products. As a contrast, we perform the similar comparison for the original real-time kinematic orbits, which can be regarded as a reference to indicate the orbit accuracy improvement brought by the proposed model.

Besides, we also employ the indicator  $P$ , a ratio between the sum of absolute differences between true results and forecast results from the BPNN model, and the sum of absolute values of true results, to evaluate the model performance as follows:

$$P = \frac{\sum |e_{\text{true}} - e_{\text{forecast}}|}{\sum |e_{\text{true}}|} \quad (7)$$

where  $e_{\text{true}}$  represents true orbit errors of LEO satellite.  $e_{\text{forecast}}$  denotes forecast orbit errors from the BPNN model. Obviously,  $P$  indicates the consistency of true orbit errors and forecast results. A smaller value of indicator  $P$  demonstrates a better performance of the method.

## III. DATASETS AND PROCESSING STRATEGIES

### A. Construction of Datasets

The datasets in this study cover a one-year period from day of year (DOY) 001 in 2022 to DOY 365 in 2022. They are based on onboard GNSS observations from six typical LEO satellites of three missions as displayed in Table II. The orbit altitude of these six LEO satellites varies from 460 to 1336 km and the orbit inclination varies from 66° to 98°. This allows

TABLE II  
INFORMATION OF SIX LEO SATELLITES FOR EXPERIMENTS

Mission	Satellite/Abbreviation	Altitude/km	Inclination/°
Swarm	Swarm-A/SWAA	460	87
	Swarm-B/SWAB	530	87
	Swarm-C/SWAC	460	87
Sentinel-3	Sentinel-3A/SE3A	814	98
	Sentinel-3B/SE3B	814	98
Sentinel-6	Sentinel-6A/SE6A	1336	66

for a comprehensive assessment of the method applicability on different LEO satellites. For Swarm and Sentinel-3 missions, a dual-frequency GPS receiver has been equipped for collecting GPS phase and code observations [29], [30]. Differently, a dual-constellation GNSS receiver (GPS+Galileo) is mounted on Sentinel-6A satellite for supporting its precise orbit determination [13]. This offers us a great chance to assess the performance of our method not only in single-GNSS solution but also in multi-GNSS solution.

Based on these collected onboard GNSS observations and GNSS real-time ephemerides, the KRTPOD of LEO satellites can be performed as described in Section II. The epochwise solution of the estimator generates both LEO real-time coordinates and multiple features as listed in Table I. The targets of the trained model are orbit errors in three axes, namely “PX\_error,” “PY\_error,” and “PZ\_error.” Note that the reference frame concerning all coordinates or coordinate corrections has been uniformly converted to the terrestrial reference system (TRS).

### B. Feature Selection

Excessive features in machine learning model training might lead to overfitting problems and increase the computational complexity and training time. Our datasets include 23 features, which may be overabundant for the BPNN model, thus leading to the performance degradation. It is, therefore, essential to implement feature selection to discard redundant features and obtain the most informative ones.

We first employ the extreme gradient boosting (XGBoost) model, a scalable machine learning system of tree boosting proposed by Chen and Guestrin [31], to evaluate the contribution of each feature to orbit errors. Fig. 2 illustrates the importance scores of all features with respect to orbit errors of Sentinel-6A satellite in three directions (“PX\_error,” “PY\_error,” “PZ\_error”). Note that the feature scores have been normalized to a scale from 0 to 1. We can see that the former three features with the greatest contribution to “PX\_error,” “PY\_error,” and “PZ\_error” are (“Epo,” “dX,” “Sig0”), (“dY,” “Epo,” “Sig0”), and (“dZ,” “Epo,” “Sig0”), respectively. It suggests that the estimated corrections of LEO orbits, the estimation time, and the MSE of unit weight can to a large extent reflect the orbit errors in each direction. Some features such as “QXX” and “QYY” exhibit insignificant contribution to orbit errors and will be discarded. Overall, the ranking results of features present the notable difference

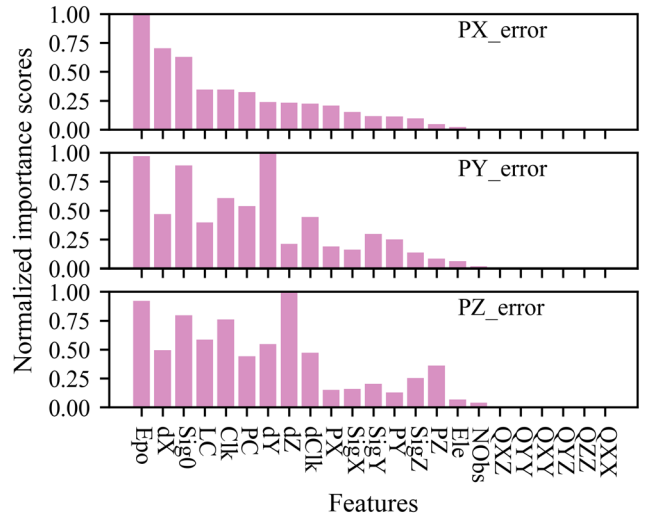


Fig. 2. Normalized feature importance scores with respect to orbit errors of Sentinel-6A satellite in three directions.

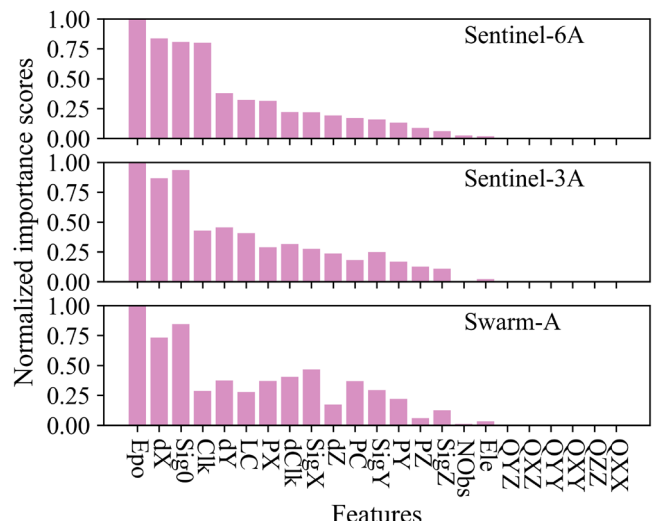


Fig. 3. Normalized feature importance scores with respect to orbit errors “PX error” for three LEO satellites.

in three directions. We therefore adopt a specific feature collection in each direction according to the corresponding feature sensitivity.

Considering that our experiments involve multiple LEO satellites, we also compare the feature importance ranking for different LEO satellites. Fig. 3 depicts the feature importance scores with respect to orbit errors “PX\_error” for Swarm-A, Sentinel-3A, and Sentinel-6A. Despite the orbit altitude difference among these satellites, no significant difference can be observed in terms of the feature ranking. We thus apply the same feature collection for different LEO satellites in the same direction. According the feature ranking results, we will choose the former 12 features to implement the model training and forecasting in the following experiments.

### *C. Processing Strategies*

Table III displays the processing strategies applied in LEO KRTPOD and the BPNN model. We use un-differenced IF

TABLE III  
PROCESSING STRATEGIES

KRTPOD processing	
Observation	Un-differenced ionosphere-free code and phase observations
Sampling rate	30 s
Arc length	24 h
GNSS antenna PCO/PCV	Use values from igs14.atx
LEO antenna PCO/PCV	Use values from the in-flight calibration
LEO attitude	Use attitude quaternion data collected by LEO onboard star trackers
Estimator	Recursive least squares
Estimated parameters	LEO coordinates (each epoch); LEO clock offsets (each epoch); Carrier phase ambiguities (each continuous arc); Inter-system bias (constant, only for GE dual-system)
BPNN configuration	
Data splitting	70%/10%/20% for training/validation/testing
Activation function	ReLU
Loss function	RMSProp
Batch size	3200
Optimizer	MSE

code and phase observations to construct the observation equation. The sampling rate of observations is set to 30 s and the arc length is 24 h. We adopt the model values from igs14.atx to correct phase center offsets (PCOs) and phase center variations (PCVs) of GNSS transmitting antennas. For LEO antenna PCO/PCV, the in-flight re-calibrated results based on postprocessed precise orbit determination are used. We first estimate the PCO values of LEO antenna using the onboard GNSS observations. By fixing the estimated PCO results, we further calibrate the PCV of LEO antenna using the residual method as performed by Jäggi et al. [32]. Attitudes of LEO satellites are determined using attitude quaternion data collected by LEO onboard star trackers. We employ the recursive least squares estimator to estimate parameters including LEO coordinates, LEO clock offsets, carrier phase ambiguities, and intersystem bias (only for GPS+Galileo dual-system).

Datasets have been divided into three parts, wherein 70%/10%/20% of the data are used for model training/validation/testing. We employ the MSE function to compute the loss value. The rms propagation (RMSProp) optimizer [33] is adopted to calculate the gradient of the loss value with respect to weight/bias parameters in each hidden layer. The batch size is set to 3200.

#### IV. EXPERIMENTAL RESULTS

In this section, we begin by performing the optimization experiments of network architecture on different LEO satellites. Based on the optimal hyperparameters, we further

assess the performance of the new method in LEO KRTPOD with different GNSS real-time orbit/clock products. Moreover, we also conduct the generalization experiments under different scenarios to evaluate the generalization ability of our new method.

##### A. Optimization of Network Hyperparameters

The architecture of neural networks plays a crucial role in learning complex systems and generalizing to new data. As the main hyperparameters of the network architecture, the number of hidden layers and the number of neurons directly determine the forecasting performance of our new method. Therefore, it is vital to investigate the optimal configuration of the number of hidden layers and neurons.

We set the number of hidden layers to the value varying from 2 to 20 with an interval of 2. The number of neurons in the hidden layers is set from 2 to 24 (twice as much as the neuron number in the input layer) with an interval of 2. Note that this setting value just refers to the neuron number in the first hidden layer. For the subsequent hidden layers, the neuron number decreases by half each time but not less than 2 to mitigate the overfitting problem. In Fig. 4, we show the normalized  $P$  values with different hidden layers and neurons for six LEO satellites. The  $P$  values from all solutions of one LEO satellite have been normalized to [0,1]. It can be seen that the distribution of  $P$  values presents a notable variation in the horizontal direction of the map for Swarm-A satellite. The left part shows small  $P$  values, whereas the results in the right part mostly reach the maximum value. This might be understood by the overfitting problem of the model with a large number of neurons. For different numbers of hidden layers, the  $P$  values exhibit no significant difference. This implies that the increase of hidden layers will not contribute to a better forecasting performance. Despite the orbit altitude/inclination difference of these six LEO satellites, we still observe the distribution similarity of their  $P$  value maps. This might be explained by that the modeled orbit errors mainly reflect GNSS ephemeris errors. As such, the network architecture might be more related with GNSS ephemerides than LEO orbit altitude/inclination. Our results demonstrate that the optimal network architecture comprises a small number of hidden layers as well as neurons ( $\leq 10$ ), and presents little variation among different LEO satellites.

Besides the number of hidden layers and neurons, the proper training epoch is also significant for enhancing the model performance and improving the computational efficiency. Based on the optimal configuration obtained from Fig. 4, we perform the model training and validation, and show the loss values with respect to training epochs in Fig. 5. The loss value of the first epoch is around 0.013 and 0.009 for the training sets and validation sets, respectively. The increase of epochs contributes to a gradual reduction of loss values. When the epoch exceeds 10, the loss value presents little variation for both training and validation sets. It indicates that the model parameters have been trained to the optimal after ten training epochs. Therefore, a training epoch with the value of 10 is preferred in our experiments.

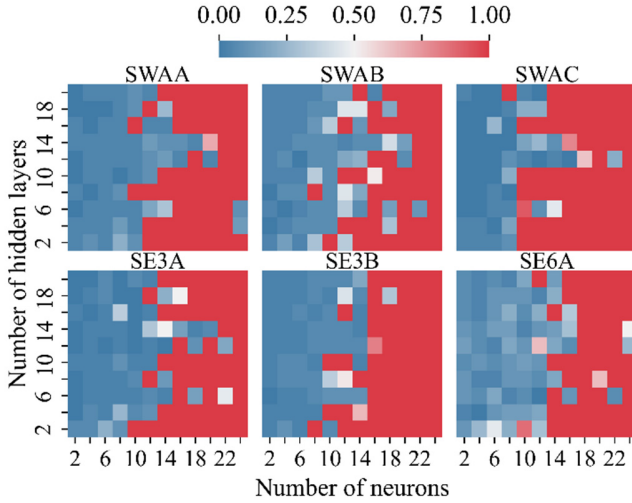


Fig. 4. Normalized results of  $P$  values from the solutions with different hidden layers and neurons for six LEO satellites.

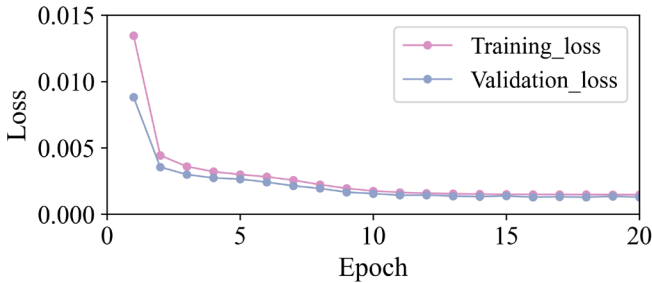


Fig. 5. Loss value per epoch during the model training and validation.

Based on these optimal network hyperparameters, we will conduct multiple experiments on different LEO satellites to assess the model performance. The model training/validation is first performed, followed by the model testing. It should be noted that we only show the results from the model testing in Sections IV-B–IV-D, and these results from the model training/validation will not be given.

### B. Results Based on GNSS Broadcast Ephemerides

In GNSS real-time applications, GNSS broadcast ephemerides are the most widely used orbit/clock products due to their convenient accessibility and negligible latency. Herein, we first utilize GNSS broadcast ephemerides to perform LEO KRTPOD for evaluating the performance of the proposed method. Fig. 6 shows the daily rms of ODs from three solutions, that is, GPS-only (G), Galileo-only (E), and GPS+Galileo (GE), for Sentinel-6A satellite. We can clearly see that the “E” solution presents a smaller daily rms of ODs than the “G” solution. This can be explained by a two-to three-times smaller signal-in-space ranging error (SISRE) of Galileo ephemerides than that of GPS ephemerides [13]. By comparison, the “GE” solution exhibits the superior performance with the smallest rms and the most stable trend. It provides evidence for the benefit of the multi-GNSS fusion in LEO KRTPOD. Overall, the results from our new method show a noticeable reduction of orbit errors compared with

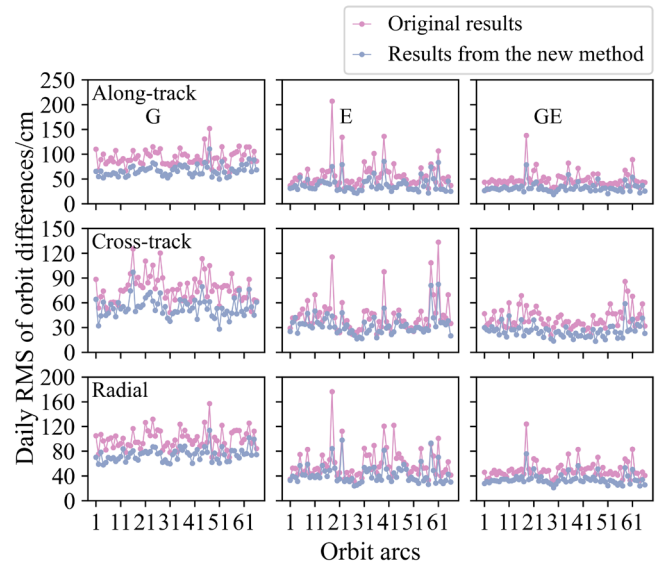


Fig. 6. Daily rms of ODs between our KRTPOD results based on GNSS broadcast ephemerides and external orbit products for Sentinel-6A satellite. “Original results” denotes the original results of LEO KRTPOD (red lines). “Results from the new method” denotes the results based on the proposed method (blue lines). The top, middle, and bottom panels show the KRTPOD results in the along-track, cross-track, and radial direction, respectively. The left, middle, and right panels show the KRTPOD results from GPS-only (G), Galileo-only (E), GPS+Galileo (GE) solution, respectively.

the original results of LEO KRTPOD. This reduction is particularly evident for some orbit arcs where the rms of original ODs is quite large for “E” and “GE” solutions. Such large orbit errors might be related with large GNSS ephemeris errors and the poor observing geometry in these days. It demonstrates that our new method can effectively improve the accuracy of LEO KRTPOD based on GNSS broadcast ephemerides especially for the lower-accuracy orbit arcs.

In Fig. 7, we show the rms of ODs between our KRTPOD results and external orbit products (left panels) and the corresponding results of  $P$  value (right panels) from six LEO satellites. The 1-D rms of original orbit errors are (91.1, 55.1, 47.0, 96.7, 96.0, 108.6, 104.4, 106.9) cm on average for Sentinel-6A(G/E/GE), Sentinel-(3A/3B), and Swarm-(A/B/C), respectively, which are reduced to (66.2, 39.0, 31.5, 69.0, 70.4, 89.8, 82.4, 87.7) cm with the application of the new method. The corresponding reduction percentages reach (27.3%, 29.2%, 33.0%, 28.6%, 26.7%, 17.3%, 21.1%, 18.0%), and the  $P$  values are (0.7, 0.7, 0.7, 0.7, 0.7, 0.8, 0.8, 0.8). The smallest mean rms around 30 cm is achieved by the “GE” solution of Sentinel-6A satellite. These results suggest that our new method can achieve the accuracy improvement of LEO KRTPOD based on GNSS broadcast ephemerides around 30% for different LEO satellites. It verifies the good performance of our new method in improving the accuracy of LEO KRTPOD.

### C. Results Based on CNES Real-Time Orbit/Clock Products

The availability of GNSS real-time orbit/clock products provided by the IGS RTS offers us a great chance to achieve

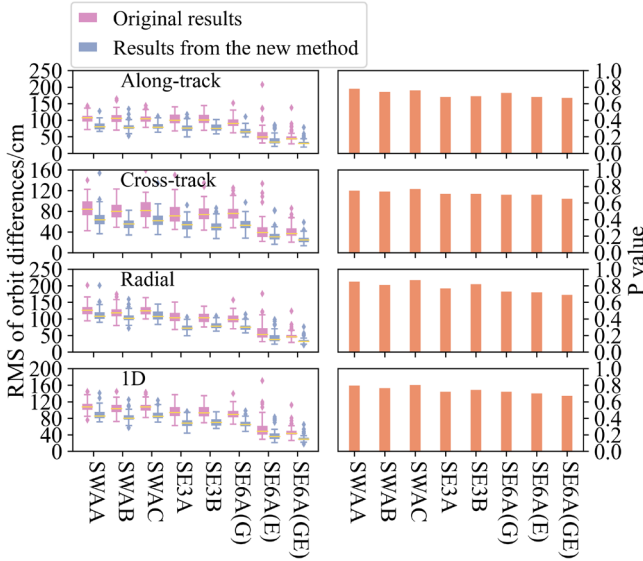


Fig. 7. Distribution of daily rms of ODs between our KRTPOD results based on GNSS broadcast ephemerides and external precise orbit products from six LEO satellites. “Original results” denotes the original results of LEO KRTPOD (red boxes). “Results from the new method” denotes the results based on the proposed method (blue boxes). The left panels show the rms of ODs in the along-track, cross-track, radial, and 1-D direction, respectively. The right panels display the corresponding results of  $P$  value.

LEO KRTPOD with centimeter-level accuracy. As one of the IGS real-time analysis centers, CNES can provide the real-time data stream as well as the archived data of orbit and clock products for GPS, Galileo, BDS, and GLONASS system [34]. We thus employ CNES real-time orbit/clock products to perform LEO KRTPOD for further examining the performance of the proposed method.

Table IV illustrates the mean and STD values of KRTPOD results based on GNSS real-time orbit/clock products from CNES for Sentinel-6A satellite. The mean values of orbit errors are approximately zero for all solutions. It implies that no evident systematic errors are existing in the results. Different from the results in the former section, the “E” solution herein presents a larger STD value of orbit errors than the “G” solution. For further investigation, we compare CNES real-time GNSS orbit products and final precise orbit products from the Center of Orbit Determination in Europe (CODE) during the testing period. Results show that the mean 1-D rms of orbit errors are 4.4 and 6.4 cm for GPS and Galileo satellites, respectively. This discrepancy can largely explain the inferior performance of the Galileo-only solution. In addition, the fewer number of available satellites per epoch for the “E” solution (5.7 on average) compared with the “G” solution (7.4 on average) also leads to a degraded accuracy. As expected, the “GE” solution exhibits the best performance due to the more available observations per epoch. The mean values are roughly zero for all solutions. In comparison with the original results, the STD values of orbit errors from our new method exhibits a smaller magnitude. This indicates the good performance of our new method in reducing orbit errors of LEO KRTPOD based on CNES real-time orbit/clock products.

TABLE IV  
MEAN AND STD VALUES OF SENTINEL-6A ODs BETWEEN OUR KRTPOD RESULTS BASED ON CNES REAL-TIME ORBIT/CLOCK PRODUCTS AND EXTERNAL PRECISE ORBIT PRODUCTS FROM ONE TYPICAL ARC (UNIT: CM)

Direction	Solution	G		E		GE	
		Mean	STD	Mean	STD	Mean	STD
Along-track	Original	0.4	5.2	0.7	8.2	0.0	3.7
	New	0.2	3.6	0.6	4.2	0.0	2.9
Cross-track	Original	0.2	4.7	0.0	5.2	0.0	3.8
	New	0.0	2.8	0.0	2.9	0.0	2.8
Radial	Original	0.0	5.4	0.0	10.7	0.0	3.3
	New	0.0	3.6	0.0	5.4	0.0	2.7

TABLE V  
MEAN VALUES OF DAILY 1-D RMS OF ODs BETWEEN OUR KRTPOD RESULTS BASED ON CNES REAL-TIME ORBIT/CLOCK PRODUCTS AND EXTERNAL PRECISE ORBIT PRODUCTS FROM SIX LEO SATELLITES (UNIT: CM)

Satellite	System	Original	New	Improvement/%	P value
Swarm-A	G	5.9	3.7	37.3	0.6
Swarm-B	G	5.1	3.2	37.3	0.6
Swarm-C	G	5.9	3.6	39.0	0.6
Sentinel-3A	G	9.0	5.7	36.7	0.6
Sentinel-3B	G	8.9	5.9	33.7	0.7
	G	7.4	4.7	36.5	0.6
Sentinel-6A	E	14.6	10.2	30.1	0.7
	GE	5.2	3.7	28.8	0.7

We further compute the statistics of the daily 1-D rms for six LEO satellites and the corresponding results of  $P$  value as depicted in Table V. The orbit accuracy improvements brought by our new method are approximately between 30% and 40% for all LEO satellites. The corresponding  $P$  values mainly vary from 0.6 to 0.7. The smallest mean 1-D rms (3.2 cm on average) is achieved by Swarm-B satellite and the most significant improvement (39.0%) is achieved by Swarm-C satellite. These promising results demonstrate that our new method can contribute to a higher accuracy of LEO KRTPOD based on precise GNSS real-time orbit/clock products. We can expect a further accuracy improvement of LEO KRTPOD brought by our new method when employing higher-accuracy real-time multi-GNSS orbit/clock products.

#### D. Generalization Tests Among Different LEO Satellites

As demonstrated in Section II, our new method employs the trained BPNN model based on the historical datasets of one LEO satellite to forecast its orbit errors. Provided that the trained BPNN model from single LEO satellite can be adopted to forecast the orbit errors of multiple LEO satellites, a large amount of computing resources can be saved and the training efficiency can also be improved significantly. This is of vital importance for a large LEO constellation with hundreds of, even thousands of satellites. It is, therefore, crucial to examine the generalization ability of our new method.

Six solutions have been designed, in which the BPNN model trained using historical data from one LEO satellite is employed to forecast orbit errors of another LEO satellite. Three scenarios are taken into consideration as follows.

1) Two LEO satellites are from one mission with the identical orbit altitude and inclination (“SWAA\_SWAC,” “SE3A\_SE3B”).

2) Two LEO satellites are from one mission but with different orbit altitudes (“SWAA\_SWAB”).

3) Two LEO satellites from different missions with different orbit altitudes and inclinations (“SWAA\_SE3A,” “SWAA\_SE6A,” “SE3A\_SE6A”). Under these scenarios, the generalization ability of our new method can be effectively examined.

In Fig. 8, we show the mean 1-D rms of orbit errors for all solutions and the corresponding  $P$  values. For scenario 1), the orbit accuracy improvement is roughly 27%, and the  $P$  value is around 0.7 for all solutions. This is reasonable because both LEO satellites orbit at an identical altitude/inclination. The orbit similarity contributes to a good generalization ability of our new method. For scenario 2), the orbit accuracy improvement brought by our new method reaches over 30% for both solutions. Despite the orbit altitude difference between Swarm-A and Swarm-B, our new method still presents superior performance. For scenario 3), we also observe the noticeable improvement of orbit accuracy roughly 30% for all solutions. This is encouraging because the trained model can be well generalized between two LEO satellites even though their orbit altitude difference reaches more than 800 km. As indicated by the aforementioned results, a key limitation to LEO KRTPOD is the accuracy of GNSS ephemerides. We thus reason that the modeled orbit errors of different LEO satellites primarily reflect GNSS ephemeris errors independent of LEO satellites. As such, with the compensation for GNSS ephemerides, the accuracy of KRTPOD for one LEO satellite can be significantly improved even using the trained model from another LEO satellite. Therefore, these findings provide evidence for the good generalization ability of our new method. This also extends the applicability of this method in the KRTPOD of future LEO constellations with thousands of satellites.

## V. DISCUSSION

Our new method presents superior performance in improving the accuracy of KRTPOD for different LEO satellites. Besides, the good generalization ability of the new method has also been verified. As indicated in Section I, LEO KRTPOD suffers from not only a lower accuracy but also a degraded robustness due to its sensitivity to GNSS ephemeris errors. We will thus evaluate the performance of the new method in improving the robustness of LEO KRTPOD in this section. Apart from these advantages, the weakness of the new method will also be discussed.

In Fig. 9, we show the daily OD between our broadcast ephemerides-based KRTPOD results and external orbit products from Sentinel-6A (top panel). A noticeable peak of orbit errors (3.2 m) can be found in the shaded part for the original results. This can be explained by the contamination of large

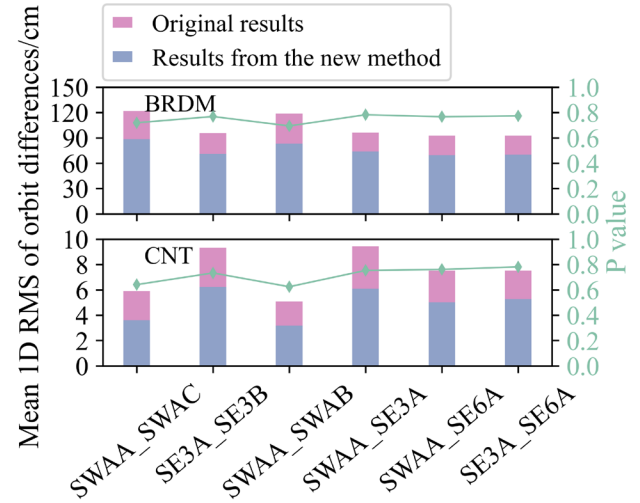


Fig. 8. Mean 1-D rms of ODs between our KRTPOD results based on GNSS broadcast ephemerides (top panel) as well as CNES real-time orbit/clock products (bottom panel) and external orbit products of different solutions and the corresponding results of  $P$  value (green lines). “Original results” denotes the original results of LEO KRTPOD (red bars). “Results from the new method” denotes the results based on the proposed method (blue bars). “LEO1\_LEO2” denotes applying the trained model from LEO1 to forecast orbit errors of LEO2.

ephemeris error from one observed GNSS satellite (E33) at the same time (middle panel). It also provides evidence for the sensitivity of LEO KRTPOD to GNSS ephemeris errors. After employing the proposed method, the corresponding orbit errors get reduced significantly to 1.5 m and no peak is observed. Such a reduction can be explained by the sensitivity of some features such as “dClk” to large GNSS ephemeris errors (bottom panel). The modeled orbit errors, therefore, can reflect such contamination. These findings demonstrate that the proposed method can remarkably improve the robustness of LEO KRTPOD by mitigating the contamination caused by large GNSS ephemeris errors.

Fig. 10 depicts the daily ODs between our KRTPOD results and external orbit products from Sentinel-6A (top panels). We can clearly see a large peak of orbit errors in the shaded part (beginning of the orbit arc), representing that the position errors have not been converged. The convergence time is 53 min for the broadcast-ephemerides-based solution and 12 min for the CNES-products-based solution. This might be related with the inaccuracy of the initial positions. By employing our new method, the convergence time is shortened to a value less than 2 min for both solutions. Similarly, such improvement can be attributed to the sensitivity of some features (“dX” and “dClk”) to orbit errors during the unconverging period (bottom panels). These results provide evidence that our new method can significantly accelerate convergence of LEO KRTPOD.

The aforementioned results demonstrate the superior performance of our new method in improving the robustness of LEO KRTPOD. The robustness herein specifically refers to the estimator-independent ability of providing accurate and stable positions even with some inevitable disturbances. For instance, the inaccuracy of initial positions will lead to a long convergence time that cannot be significantly shortened by the

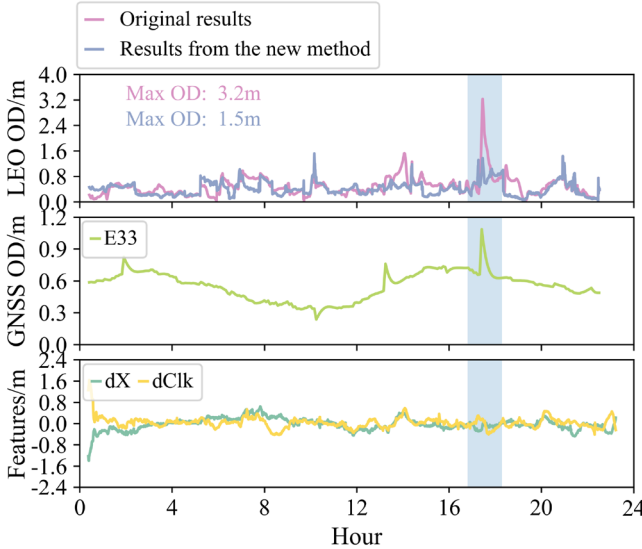


Fig. 9. ODs between our broadcast-ephemerides-based KRTPOD results and external orbit products from Sentinel-6A (top panel), ODs between broadcast ephemerides and final precise orbit products from E33 (middle panel), and the results of two typical features (“dX” and “dClk”) (bottom panel), on DOY 298 in 2022.

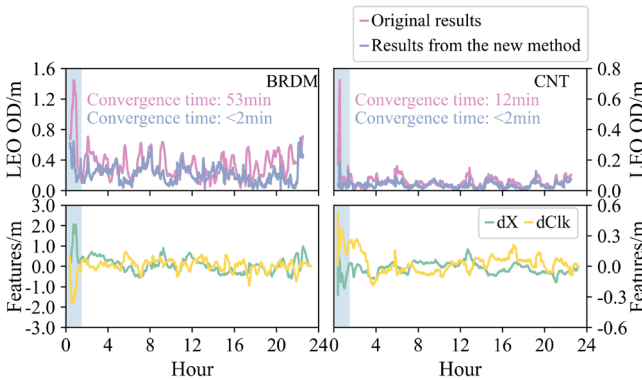


Fig. 10. ODs between our KRTPOD results and external orbit products from Sentinel-6A (top panels) and the results of two typical features (“dX” and “dClk”) (bottom panels). The left panels show the broadcast-ephemerides-based results (BRDM) on DOY 310 in 2022 and the right panels show the CNES-products-based results (CNT) on DOY 293 in 2022.

adoption of different estimator. In addition, provided that the ephemeris errors of all the observed GNSS satellites are large in some epochs, the KRTPOD results may not remain accurate even with a more robust estimator. Therefore, our new method has the great potential of improving the robustness of LEO KRTPOD.

Given that a major advantage of LEO KRTPOD is the low computational resources, one may be more concerned with how much the computational resources are consumed for this method. Table VI displays the computational resource consumption of the BPNN model in the KRTPOD of Sentinel-6A satellite. The total time consumption is 204 s for model training with 507 059 samples. By comparison, the total consumed time for forecasting 144 870 samples is only 10 s. It indicates that forecasting the orbit errors of one epoch requires an insignificant time cost less than  $10^{-4}$  s, allowing for a compensation for LEO orbits with no latency.

TABLE VI  
COMPUTATIONAL RESOURCE CONSUMPTION OF THE BPNN  
MODEL FOR SENTINEL-6A SATELLITE

Description	Model training	Model testing
Number of Samples	507059	144870
Total time consumption	204 s	10 s
Running memory	496 Mb	175 Mb
Storage memory of model	4 Kb	----

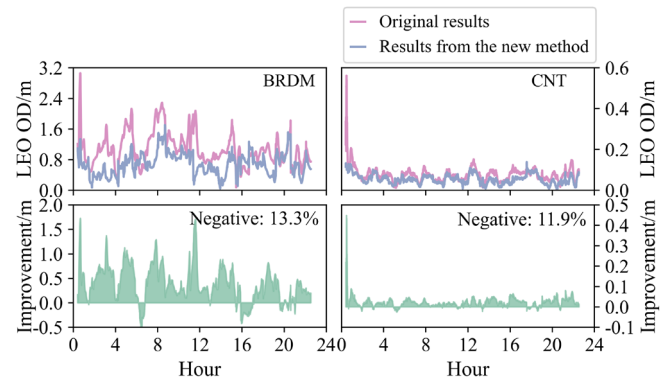


Fig. 11. ODs between our KRTPOD results and external orbit products from Sentinel-6A (top panels) and the corresponding accuracy improvement (bottom panels). The left panels show the broadcast-ephemerides-based results (BRDM) on DOY 316 in 2022, and the right panels show the CNES-products-based results (CNT) on DOY 303 in 2022.

Considering that the training processing is based on historical datasets that demand external precise orbit products, we can carry out the model training every several days or weeks in practical applications to update the BPNN model. The running memory is 496 Mb for the model training and 176 Mb for the model testing. The size of the trained model that contains all optimal weight/bias parameters is around 4 Kb. Such a minimal storage memory makes this method well suited for onboard processing.

In Fig. 11, we show the orbit errors of Sentinel-6A (top panels) and the corresponding improvement (bottom panels) for both broadcast-ephemerides-based and CNES-products-based solutions. Overall, the new method can contribute to the orbit accuracy improvement in most epochs. We also notice, nonetheless, some negative improvements for both solutions. The percentage of negative values is 13.3% for the broadcast-ephemerides-based solution and 11.9% for the CNES-products-based solution. As indicated in Section II, the model training is aimed at establishing the mapping relationship between the input features and the output orbit errors as accurately as possible. Our feature sets, however, may be imperfect due to the lack of more features strongly related with orbit errors. As a result, the modeled orbit errors suffer from uncertainties. When the original orbit errors are of large magnitude, the impact caused by such uncertainties is obscured. This can largely explain the notable positive improvement when the original orbit errors are large. On the contrary, for these epochs with small orbit errors, the negative impact caused by the modeling uncertainties is revealed.

This leads to the negative values of accuracy improvement. To overcome this weakness, it is recommended that more features strongly related with orbit errors should be introduced into the model training. Besides, the ongoing advancement in machine learning technology might also contribute to the solution of this problem.

## VI. CONCLUSION

The traditional KRTPOD of LEO satellites is sensitive to GNSS ephemeris errors and observation geometry/quality due to the sole use of onboard GNSS observations. This leads to a degraded accuracy and robustness of LEO real-time orbits. To address this issue, we propose a novel method where the BPNN model is introduced into LEO KRTPOD to improve its accuracy and robustness. Historical multiple features and orbit errors of LEO KRTPOD serve as the input and output of the BPNN model, respectively, for the training purpose. During the processing of LEO KRTPOD, the real-time orbits are computed. Meanwhile, the epochwise multiple features are generated and then conveyed to the trained model for forecasting orbit errors. The forecast orbit errors are subsequently used to compensate for LEO real-time orbits with the aim of enhancing its accuracy and robustness. Datasets of six LEO satellites from DOY 001 in 2022, to DOY 365 in 2022 are processed to examine the performance of the proposed method.

We begin by conducting the optimization experiments of the network architecture on different LEO satellites. Results demonstrate that the optimal network architecture comprises a small number of hidden layers as well as neurons ( $\leq 10$ ) and presents little variation among different LEO satellites. Based on the optimal configuration, we perform LEO KRTPOD using GNSS broadcast ephemerides. Our findings reveal that the new method can significantly improve the orbit accuracy. The orbit accuracy improvement is 17%–35%. The corresponding  $P$  value varies from 0.6 to 0.8. We additionally employ CNES real-time orbit/clock products to conduct the experiments. The results indicate that the orbit accuracy improvement brought by our new method reaches 30%–40%. The corresponding  $P$  value varies from 0.6 to 0.7. Benefiting from the new method, the orbit accuracy of 3.2 cm can be obtained in LEO KRTPOD. These results demonstrate the good performance of our new method in improving the accuracy of LEO KRTPOD. Generalization tests under different scenarios demonstrate that our new method can be well generalized to different LEO satellites even with different orbit altitudes/inclinations. The orbit accuracy improvement can still reach approximately 30% for one LEO satellite when using the trained model from another LEO satellite.

We also demonstrate that the new method can enhance the robustness of LEO KRTPOD by significantly mitigating the contamination caused by large GNSS ephemeris errors and remarkably shortening the convergence time. A fast speed of model forecasting allows for the real-time compensation for orbit errors. A minimal storage memory around 4.0 Kb of the trained model makes this method well suited for onboard processing. In addition, we also reveal a drawback of the new method that negative improvement might occur when the original orbit errors are small. This weakness might be

overcome by the introduction of more features that are strongly correlated with orbit errors and the continuous advancement in machine learning technology.

With the application of the basic BPNN model, we have demonstrated the great potential of neural networks in improving the accuracy and robustness of LEO KRTPOD. Future work can be extended to the employment of more neural network models and the comparison between different models. Besides, we will introduce more features strongly related with orbit errors into the modeling to reduce negative improvements. As such, more contribution of neural networks to LEO KRTPOD can be expected.

## ACKNOWLEDGMENT

The numerical calculations in this article have been done on the supercomputing system in the Supercomputing Center of Wuhan University.

## REFERENCES

- [1] M. Ge, G. Gendt, M. Rothacher, C. Shi, and J. Liu, “Resolution of GPS carrier-phase ambiguities in precise point positioning (PPP) with daily observations,” *J. Geodesy*, vol. 82, no. 7, p. 401, Jul. 2008.
- [2] X. Li, Y. Yuan, X. Han, X. Li, and Y. Fu, “Toward wide-area and high-precision positioning with LEO constellation augmented PPP-RTK,” *IEEE Trans. Instrum. Meas.*, vol. 73, 2023, Art. no. 5500213.
- [3] X. Li, X. Li, Y. Yuan, K. Zhang, X. Zhang, and J. Wickert, “Multi-GNSS phase delay estimation and PPP ambiguity resolution: GPS, BDS, GLONASS, Galileo,” *J. Geodesy*, vol. 92, no. 6, pp. 579–608, Jun. 2018.
- [4] P. Enge, B. Ferrell, J. Bennett, D. Whelan, G. Gutt, and D. Lawrence, “Orbital diversity for satellite navigation,” in *Proc. 25th Int. Tech. Meeting, Satell. Division Inst. Navigat. (ION GNSS)*, 2012, pp. 3834–3846.
- [5] T. G. Reid, A. M. Neish, T. F. Walter, and P. K. Enge, “Leveraging commercial broadband leo constellations for navigating,” in *Proc. 29th Int. Tech. Meeting Satell. Division Inst. Navigat. (ION GNSS+)*, Nov. 2016, p. 2016.
- [6] X. Mao, P. N. A. M. Visser, and Jose van den IJssel, “Absolute and relative orbit determination for the CHAMP/GRACE constellation,” *Adv. Space Res.*, vol. 63, no. 12, pp. 3816–3834, Jun. 2019.
- [7] K. Zhang et al., “Precise orbit determination for LEO satellites with ambiguity resolution: Improvement and comparison,” *J. Geophys. Res., Solid Earth*, vol. 126, no. 9, Aug. 2021, Art. no. e2021JB022491.
- [8] S. C. Wu, T. P. Yunck, and C. L. Thornton, “Reduced-dynamic technique for precise orbit determination of low earth satellites,” *J. Guid., Control, Dyn.*, vol. 14, no. 1, pp. 24–30, Jan. 1991.
- [9] O. Montenbruck, T. van Helleputte, R. Kroes, and E. Gill, “Reduced dynamic orbit determination using GPS code and carrier measurements,” *Aerospace Sci. Technol.*, vol. 9, no. 3, pp. 261–271, Apr. 2005.
- [10] Y. Yang, X. Yue, and A. G. Dempster, “GPS-based onboard real-time orbit determination for leo satellites using consider Kalman filter,” *IEEE Trans. Aerosp. Electron. Syst.*, vol. 52, no. 2, pp. 769–777, Apr. 2016.
- [11] A. Hauschild and O. Montenbruck, “Precise real-time navigation of LEO satellites using GNSS broadcast ephemerides,” *Navigation*, vol. 68, no. 2, pp. 419–432, Jun. 2021.
- [12] F. Wang, X. Gong, J. Sang, and X. Zhang, “A novel method for precise onboard real-time orbit determination with a standalone GPS receiver,” *Sensors*, vol. 15, no. 12, pp. 30403–30418, Dec. 2015.
- [13] O. Montenbruck, F. Kunz, and A. Hauschild, “Performance assessment of GNSS-based real-time navigation for the Sentinel-6 spacecraft,” *GPS Solutions*, vol. 26, p. 12, Nov. 2021.
- [14] T. Hadad and J. Bosy, “IGS RTS precise orbits and clocks verification and quality degradation over time,” *GPS Solutions*, vol. 19, no. 1, pp. 93–105, Feb. 2014.
- [15] M. Wermuth, A. Hauschild, O. Montenbruck, and R. Kahle, “TerraSAR-X precise orbit determination with real-time GPS ephemerides,” *Adv. Space Res.*, vol. 50, no. 5, pp. 549–559, Sep. 2012.
- [16] Z. Wang et al., “Comparison of the real-time precise orbit determination for LEO between kinematic and reduced-dynamic modes,” *Measurement*, vol. 187, Jan. 2022, Art. no. 110224.

- [17] G. Allende-Alba, O. Montenbruck, J. S. Ardaens, M. Wermuth, and U. Hugentobler, "Estimating maneuvers for precise relative orbit determination using GPS," *Adv. Space Res.*, vol. 59, no. 1, pp. 45–62, Jan. 2017.
- [18] D. Švehla and M. Rothacher, "Kinematic and reduced-dynamic precise orbit determination of low Earth orbiters," *Adv. Geosci.*, vol. 1, no. 1, pp. 47–56, Jun. 2003.
- [19] U. Weinbach and S. Schön, "Improved GRACE kinematic orbit determination using GPS receiver clock modeling," *GPS Solutions*, vol. 17, no. 4, pp. 511–520, Nov. 2012.
- [20] P. Chen, J. Zhang, and X. Sun, "Real-time kinematic positioning of LEO satellites using a single-frequency GPS receiver," *GPS Solutions*, vol. 21, no. 3, pp. 973–984, Nov. 2016.
- [21] X. Li, J. Wu, K. Zhang, X. Li, Y. Xiong, and Q. Zhang, "Real-time kinematic precise orbit determination for LEO satellites using zero-differenced ambiguity resolution," *Remote Sens.*, vol. 11, no. 23, p. 2815, Nov. 2019.
- [22] G.-B. Huang, H. Zhou, X. Ding, and R. Zhang, "Extreme learning machine for regression and multiclass classification," *IEEE Trans. Syst., Man, Cybern., B (Cybern.)*, vol. 42, no. 2, pp. 513–529, Apr. 2012.
- [23] A. Bernieri, L. Ferrigno, M. Laracca, and M. Molinara, "Crack shape reconstruction in eddy current testing using machine learning systems for regression," *IEEE Trans. Instrum. Meas.*, vol. 57, no. 9, pp. 1958–1968, Sep. 2008.
- [24] R. Hecht-Nielsen, "Theory of the backpropagation neural network," *Neural Netw.*, vol. 1, p. 445, Jan. 1998.
- [25] T. C. Goh, "Back-propagation neural networks for modeling complex systems," *Artif. Intell. Eng.*, vol. 9, no. 3, pp. 143–151, 1995.
- [26] G. Blewitt, "An automatic editing algorithm for GPS data," *Geophys. Res. Lett.*, vol. 17, no. 3, pp. 199–202, Mar. 1990.
- [27] X. Li et al., "Multi-GNSS products and services at iGMAS Wuhan Innovation Application Center: Strategy and evaluation," *Satell. Navigat.*, vol. 3, p. 20, Sep. 2022.
- [28] X. Glorot, A. Bordes, and Y. Bengio, "Deep sparse rectifier neural networks," in *Proc. 14th Int. Conf. Artif. Intell. Statist. (AISTATS)*, vol. 15, 2011, pp. 315–323.
- [29] E. Friis-Christensen, H. Lühr, D. Knudsen, and R. Haagmans, "Swarm—An Earth observation mission investigating geospace," *Adv. Space Res.*, vol. 41, no. 1, pp. 210–216, 2008.
- [30] K. Fletcher, Ed., *Sentinel-3-ESA's Global Land and Ocean Mission for GMES Operational Services*. Noordwijk, The Netherland: ESA Special Publication (SP-1322/3), Oct. 2012.
- [31] T. Chen and C. Guestrin, "XGBoost: A scalable tree boosting system," in *Proc. 22nd ACM SIGKDD Int. Conf. Knowl. Discovery Data Mining*, Aug. 2016, pp. 785–794.
- [32] A. Jäggi, R. Dach, O. Montenbruck, U. Hugentobler, H. Bock, and G. Beutler, "Phase center modeling for LEO GPS receiver antennas and its impact on precise orbit determination," *J. Geodesy*, vol. 83, no. 12, pp. 1145–1162, Jul. 2009.
- [33] A. Graves, "Generating sequences with recurrent neural networks," 2013, *arXiv:1308.0850*.
- [34] D. Laurichesse, L. Cerri, J. P. Berthias, and F. Mercier, "Real time precise GPS constellation and clocks estimation by means of a Kalman filter," in *Proc. 26th Int. Tech. Meeting Satell. Division Inst. Navigat. (ION-GNSS)*, Sep. 2013, pp. 1155–1163.



**Keke Zhang** is currently a Post-Doctoral Researcher with Wuhan University, Wuhan, China. His area of research currently focuses on the integrated orbit determination of low Earth orbit (LEO) and global navigation satellite system (GNSS) satellites and geodetic parameter estimation with LEO-based observations.



**Xingxing Li** received the Ph.D. degree from the Department of Geodesy and Remote Sensing, German Research Centre for Geosciences (GFZ), Potsdam, Germany, in 2015.

He is currently a Professor with Wuhan University, Wuhan, China. His current research mainly involves global navigation satellite system (GNSS) precise data processing and its application for geosciences.



**Jiaqi Wu** is currently pursuing the Ph.D. degree with Wuhan University, Wuhan, China.

His area of research currently focuses on the ambiguity-fixed resolution in the precise orbit determination of global navigation satellite system (GNSS) satellites.



**Yongqiang Yuan** is currently a Post-Doctoral Researcher with Wuhan University, Wuhan, China. His area of research currently focuses on the precise orbit determination of global navigation satellite system (GNSS) satellites and the refinement of the nonconservative force model.



**Wei Zhang** is currently pursuing the Ph.D. degree with Wuhan University, Wuhan, China.

His research currently focuses on the precise orbit determination of low Earth orbit (LEO) satellites and LEO orbit and clock prediction with machine learning methods.



**Yuanchen Fu** is currently pursuing the master's degree with Wuhan University, Wuhan, China.

His current research focuses on precise orbit determination of global navigation satellite system (GNSS) and low Earth orbit (LEO) satellites.